ITERATIVE DEBLENDING BASED ON THE MODIFIED SINGULAR SPECTRUM ANALYSIS

JUAN WU and MIN BAI

Key Laboratory of Exploration Technology for Oil and Gas Resources of the Ministry of Education, Yangtze University, Wuhan 430100, P.R. China. wujuan_2016@126.com

(Received February 18, 2018; revised version accepted October 7, 2018)

ABSTRACT

Wu, J. and Bai, M., 2019. Iterative deblending based on the modified singular spectrum analysis. *Journal of Seismic Exploration*, 28: 1-20.

Deblending of simultaneous-source seismic data aims at separating the blended records caused by simultaneous shooting as if the data are acquired traditionally. In this paper, we propose a novel modified singular spectrum analysis (SSA) approach to remove blending noise in an iterative inversion manner. Compared with the traditional SSA approach, the modified SSA approach applies a modified truncated singular value decomposition (TSVD) onto the Hankel matrix in the frequency domain, and can attenuate more blending noise than the traditional SSA method. We use both synthetic and field data examples to demonstrate that the proposed modified SSA method has a stronger signal-and-noise separability.

KEY WORDS: deblending, singular value decomposition, noise, singular spectrum analysis, iterative solver.

INTRODUCTION

Modern seismic acquisition requires a high-density, wide-azimuth coverage for improving the subsurface illumination (Chen et al., 2017a,c). Large acquisition systems require a highly efficient acquisition deployment.

0963-0651/19/$5.00

The principal purpose of simultaneous source acquisition is to accelerate the acquisition of a large-density seismic dataset, which can save acquisition cost and increase data quality. The simultaneous shooting technique has existed for decades. It has raised special attention recently because of its application to marine acquisition. The benefits are compromised by the intense interference between different shots (Berkhout, 2008; Beasley, 2008; Berkhout and Blacquiere, 2013; Abma, 2014; Amundsen et al., 2018; Zu et al., 2017a). One approach to solve the problem caused by interference is by a first- separate and second-processing strategy (Mahdad, 2012; Qu et al., 2014; Wu et al., 2015; Mueller et al., 2015; Gan et al., 2016a,c), which is also called deblending. Another way is by direct imaging and inversion of the blended data via attenuating the interference during the inversion process (Verschuur and Berkhout, 2011; Zu et al., 2017b; Chen et al., 2017e; Gan et al., 2016d; Bai and Wu, 2017; Bai et al., 2018; Wu and Bai, 2018).

Some researchers have proposed various filtering methods to attenuate the interference noise, which can also be referred to as a noise reduction problem (Chen and Fomel, 2015; Huang et al., 2016, 2017b; Zhang et al., 2016, 2017). The separation methods base on inversion regard the separation processing as an estimated issue, which aim at estimating the ideal unknown unblended data by attenuating the interference noise (Huang et al., 2018b). Due to the ill-posed characteristic of inversion problems, some constraints should be added into inversion framework to make the inversion problem proper. Abma and Yan (2009) proposed a sparse constraint in f-k domain. Xue et al. (2017) used high-order radon transform to shape the inversion framework to remove the blending noise and preserve the amplitude. Chen (2017) proposed a way of fast dictionary learning to represent seismic data sparsely. The dictionary learning method can adaptively learn the basis of a sparse transform (Siahsar et al., 2017a,b). Yu et al. (2017) proposed an approach using a wavelet transform to deterministically separate the primary signal from the noise, including simultaneous source interference noise. Usually, the inversion methods perform better than the filtering methods. Xue et al. (2016) propose a rank-increasing methods for deblending via iteratively estimating the blending noise instead of the signals. Many other advanced denoising algorithms can also be used to attenuate the blending noise by simple filtering (Chen and Ma, 2014; Chen et al., 2016a; Li et al., 2016a; Chen, 2016; Li et al., 2016b; Huang et al., 2017a,c,d; Chen et al., 2017b,d; Xie et al., 2017; Chen, 2018; Chen and Fomel, 2018; Huang et al., 2018a).

Inversion based methods treat the deblending problem as an inverse problem and solve it using some iterative solvers. Low-rank based methods have been widely used in the literature for deblending. The low-rank constraint can be applied via the Cadzow filtering method (Cadzow, 1988), damped rank-reduction method (Chen et al., 2016c,d), the randomized multichannel singular spectrum analysis (RMSSA) method (Huang et al., 2017b), the adaptive damped multichannel singular spectrum analysis

(ADMSSA) (Siahsar et al., 2017c), sparsity-constrained MSSA method (Wang et al., 2017; Zhang et al., 2017), or the multi-step MSSA method (Zhang et al., 2016). Similarly, Xue et al. (2016) used the increased low-rank to separated the blended record. However, when the rank is too small at initial iteration, some unexpected noise is introduced. Zu et al. (2017c) combined the increased low-rank constraint with threshold to further improve the deblending performance. The low-rank constraint is similar to the sparsity promotion constraint, which belongs to the compressed sensing principle Gan et al. (2015); Liu et al. (2016b); Gan et al. (2016b); Liu et al. (2016a); Bai and Wu (2018); Liu et al. (2018). Zhou et al. (2018) proposed the subspace tracking based rank-reduction method. Zhou et al. (2017) used the structural rank reduction method to more or less solve the rank inconsistency problem of the local-window based rank reduction method. A similar structural smoothness constraint was used by Chen et al. (2016b) for interpolating sparsely sampled geophysical dataset. In the algorithmic aspects of inversion, Doulgeris et al. (2012) discussed the convergence properties.

In this paper, we propose a novel inversion scheme based on a modified singular spectrum analysis (SSA) algorithm. We know that the interference noise contained in simultaneous source data will increase the rank, therefore, if we can select the suitable preserved rank, then the interference noise can be removed well. However, it is not easy to set the rank, especially for the complex seismic data, which increases the rank and cause a serious rank-mixing problem. Obviously, once the rank is chosen too small, it will bring some extra unexpected information and make the signal damaged. Otherwise, the interference noise cannot be suppressed well. Our proposed method solves this problem by first setting a relatively large rank and then using a modified truncated singular value decomposition (TSVD) to attenuate those residual noise left in the Hankel matrix that is caused by the relatively large rank. In the inversion framework, the modified SSA method improves the deblending performance by better separating the blended data into signal and noise subspaces. We use two examples to compare with the traditional FX method and SSA method to validate the effectiveness of our method.

THEORY

Iterative deblending based on the shaping regularization framework

To be convenient, we assume that one simultaneous source data is blended using two independent sources, which correspond to two shooting sources in ocean bottom cable (OBC) acquisition. Therefore, the blending forward processing is done in the common-receiver domain (Chen et al., 2014),

$$d = \Gamma_1 d_1 + \Gamma_2 d_2 \quad , \tag{1}$$

where d is the blended data, d_1 and d_2 are the first and second independent receiver gathers, respectively, and Γ_1 and Γ_2 denote the dithering operators corresponding to d_1 and d_2, respectively. In the process of deblending, different phase-encoding blending operators have been introduced to eliminate the crosstalk noise, such as linear phase term and quadratic phase term. Here, the linear phase encoding that expresses the time delays in the time domain was applied (Zu et al., 2016b; Qu et al., 2015, 2016). The blending operator can be written as the following form,

$$\Gamma_i = F^{-1} P_i F \quad , \qquad \text{for } i = 1, 2, \tag{2}$$

$$P_i = \mathrm{diag}(e^{-jwt_{i,1}}, e^{-jwt_{i,2}}, \cdots, e^{-jwt_{i,m}}) \quad , \tag{3}$$

where Γ_i is the dithering operator of the i-th common-receiver record in the time domain, P_i represents the phase matrix of the i-th common-receiver record, $t_{i,m}$ is the delay time for the m-th trace of the i-th common-receiver record, w is the angular frequency, and j represents the imaginary unit. Note that we use the random time delay in this paper.

Eq. (1) can be expressed into a matrix-vector multiplication form as

$$d = \Gamma m, \tag{4}$$

where

$$\Gamma = \begin{bmatrix} \Gamma_1 & \Gamma_2 \end{bmatrix} \quad , \tag{5}$$

and

$$\mathbf{m} = \begin{bmatrix} \mathbf{d}_1 \\ \mathbf{d}_2 \end{bmatrix} \quad . \tag{6}$$

d is the blended data, Γ is the blending operator, and **m** is the unblended data. The formulation of Γ has been introduced in Mahdad (2012) in detail. When considered in time domain, Γ corresponds to blending different shot records onto one receiver record according to the shot schedules of different shots. Deblending amounts to inverting eq. (4) and recovering **m** from **d**.

Because of the ill-posed property of this problem, all inversion methods require some constraints. Chen et al. (2014) proposed a general iterative deblending framework via shaping regularization (Fomel, 2007, 2008; Zu et al., 2016a). The iterative deblending is expressed as:

$$m_{n+1} = S[m_n + B[d - \Gamma m_n]] \quad , \tag{7}$$

where S is the shaping operator, which provides some constraints on the model, and B is the backward operator, which approximates the inverse of Γ. The shaping regularization framework offers us much freedom in constraining an under-determined problem by allowing different types of constraints. In this paper, the backward operator is simply chosen as $\lambda\Gamma^*$, where λ is a scale coefficient closely related with the blending fold, and Γ^* stands for the adjoint operator of Γ (or the pseudo-deblending operator). For example, λ can be optimally chosen as 1/2 in a two-source dithering configuration (Chen et al., 2014; Mahdad, 2012). In this paper, S is chosen as the modified SSA operator, which will be introduced in detail next.

Singular spectrum analysis

In the case of a 2D seismic record D(x,t), we carry out Fourier transform on the data *f* (*x, t*) represented as *F* (*x, w*), then for each frequency slice *F* (*x, w*), the Hankel matrix can be written as **M**:

$$\begin{aligned}\mathbf{M} &= \mathcal{HF}[D(x,t)] \\ &= \begin{pmatrix} D(1,w) & D(2,w) & \cdots & D(K,w) \\ D(2,w) & D(3,w) & \cdots & D(K+1,w) \\ \vdots & \vdots & \ddots & \vdots \\ D(L,w) & D(L+1,w) & \cdots & D(M,w) \end{pmatrix},\end{aligned} \tag{8}$$

where *t* denotes time, *w* denotes frequency. **M** denotes the total number of traces, *H* denotes the Hankel matrix, *F* is the Fourier transform operator.

L = $\lfloor^{M}\rfloor$+1 and K = M –L+1, and $\lfloor\cdot\rfloor$ denotes the integer part of its argument. If the seismic data contains k linear events, then the rank of Hankel matrix **M** is k. The interference noise existing in the blended records will make the Hankel matrix rank raising. Therefore, the problem of deblending can be regarded as a rank-reduction problem. It will be beneficial to apply truncated singular value decomposition (TSVD) to the Hankel matrix to estimate signals (Huang et al., 2016). Then the estimated signals can be reconstructed by averaging components of the processed Hankel matrix. We can represent the whole process of SSA algorithm as follows:

$$\hat{D}(x,t) = \mathcal{F}^{-1}\mathcal{ARHF}[D(x,t)] = \mathcal{P}D(x,t) \quad , \tag{9}$$

where F^{-1} indicates the inverse Fourier transform, A indicates the averaging operator, the R denotes the TSVD operator, and $P = F^{-1}ARHF$ indicates a combined rank-reduction operator (i.e., the SSA operator).

Modified singular spectrum analysis

In eq. (8), the Hankel matrix **M** can be represented as:

$$\mathbf{M} = \mathrm{S} + \mathrm{N} \quad , \tag{10}$$

where S and N denote the block Hankel matrix of signal and of random noise, respectively.

We assume that **M** and N have full rank, rank(M) = rank(N) = J and S has deficient rank, rank(S) = K < J. The singular value decomposition (SVD) of M can be represented as:

$$\mathbf{M} = [\mathbf{U}_1^M \quad \mathbf{U}_2^M] \begin{bmatrix} \Sigma_1^M & \mathbf{0} \\ \mathbf{0} & \Sigma_2^M \end{bmatrix} \begin{bmatrix} (\mathbf{V}_1^M)^H \\ (\mathbf{V}_2^M)^H \end{bmatrix} \quad , \tag{11}$$

where $\Sigma^{\mathrm{M}}{}_1$ respectively, larger singular values and smaller singular values.

$\mathrm{U}^{\mathrm{M}}{}_1$ (I × K), $\mathrm{U}^{\mathrm{M}}{}_2$ (I × (I − K)), $\mathrm{V}_1{}^{\mathrm{M}}$ (J × K) and $\mathrm{V}_2{}^{\mathrm{M}}$ (J × (J − K)) denote the associated matrices with singular vectors. The symbol $[\cdot]^{\mathrm{H}}$ denotes the conjugate transpose of a matrix. In general the signal is more energy-concentrated and correlative than the random noise. Thus, the larger singular values and their associated singular vectors represent the signal, while the smaller values and their associated singular vectors represent the random noise. We let $\Sigma^{\mathrm{M}}{}_2$ be 0 to achieve the goal of attenuating random noise while recovering the missing data during the first iteration in reconstruction process as follows:

$$\tilde{\mathbf{M}} = \mathbf{U}_1^M \Sigma_1^M (\mathbf{V}_1^M)^H \quad . \tag{12}$$

Eq. (12) is referred to the TSVD, which is used in the conventional SSA approach.

However, **M** is actually still contaminated with residual blending noise. Huang et al. (2015) derived a modified TSVD algorithm to attenuate the residual noise caused by the conventional SSA. Here, we further apply the TSVD algorithm to simultaneous data separation, and

apply the modified TSVD algorithm iteratively for constraining the model when solving the blending equation. It can be derived that approximation of **S** can be expressed:

$$\mathbf{S} = \mathbf{U}_1^M \Sigma_1^M \mathbf{T} (\mathbf{V}_1^M)^H \quad , \tag{13}$$

$$\mathbf{T} = \mathbf{I} - (\Sigma_1^M)^{-N} \hat{\delta}^N \quad , \tag{14}$$

where $\hat{\delta}$ denotes the maximum element of Σ^{M}_{2} and N denotes the control factor. It is worth mentioning that the greater the N, the weaker the damping, and eq. (13) degrades to eq. (12) when $N \rightarrow +\infty$.

The revised TSVD for the SSA algorithm can be represented in operator notation as follows:

$$\mathbf{S} = \mathrm{R_m}\mathbf{M} \quad , \tag{15}$$

where we use $\mathrm{R_m}$ as the rank reduction operator for the modified SSA while R is used for conventional SSA, as shown in eq. (9).

EXAMPLES

In this section, we use one synthetic and one field data examples to demonstrate the performance of the proposed method based on the iterative framework expressed in eq. (7). We use two simultaneous sources in the numerical tests. Being concise, we only show the deblending performance of one record and omit the performance from the other source since the two common receiver records that are used for the blending are very similar. To quantitatively measure the deblending performance, we use the metric (signal-to-noise ratio; *SNR*) defined in Chen et al. (2014):

$$SNR_n = 10 \log_{10} \frac{\|\mathbf{m}_0\|_2^2}{\|\mathbf{m}_0 - \mathbf{m}_n\|_2^2} \quad , \tag{16}$$

where SNR_n denotes the *SNR* after *n* iterations, $\mathbf{m}_0$ denotes the clean unblended data and m_n denotes the deblended data after *n* iterations.

The first example is shown in Fig. 1. Fig. 1(a) shows the clean data and Fig. 1(b) shows the blended data, which is contaminated by strong spiky-like blending interference. In this example, the blending fold is 3. Figs. 1(c) and 1(d) show two zoomed areas from Figs. 1(a) and 1(b). The zooming areas are highlighted by the two black frame boxes in Figs. 1(a) and 1(b).

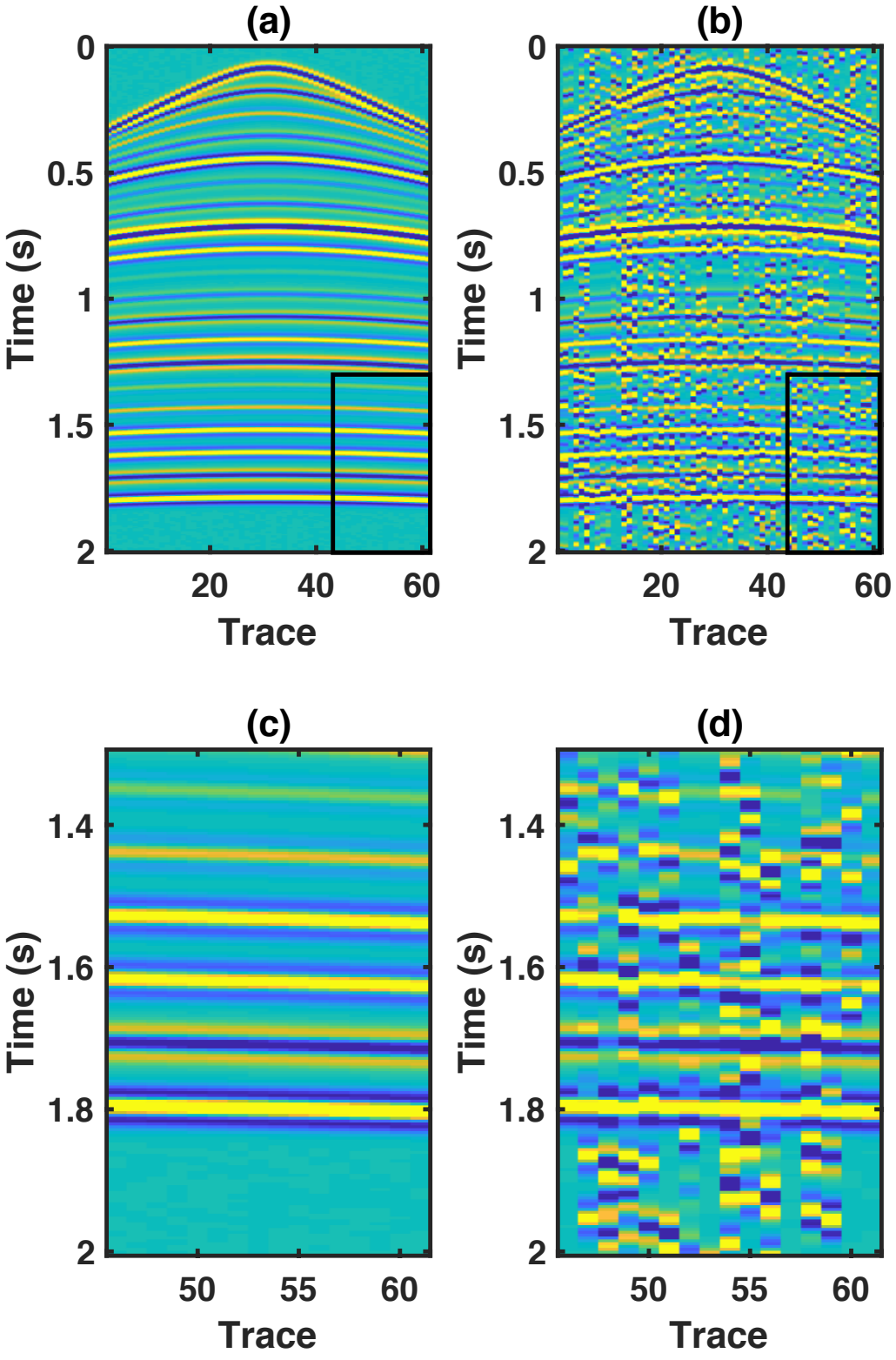

Fig. 1. Synthetic example. (a) Clean data. (b) Blended data. (c) Zoomed (a). (d) Zoomed (b).

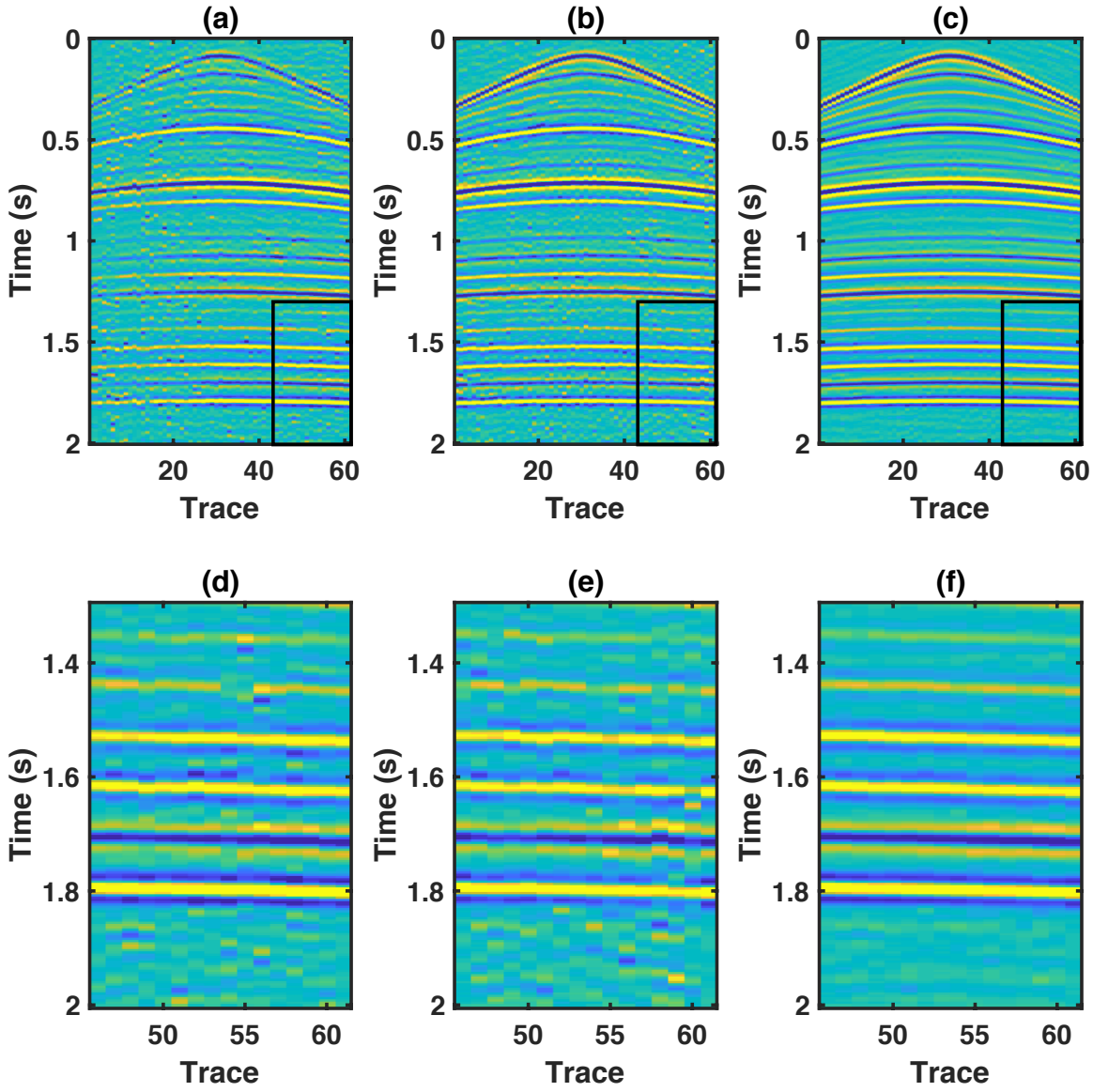

Fig. 2. Synthetic example. (a) Deblended data using FX method. (b) Deblended data using SSA method. (c) Deblended data using the proposed method. (d)-(f) Zoomed areas corresponding to the frameboxes in (a)-(c). Note that the proposed method obtains the cleanest result.

Fig. 2 shows the deblending performance using three different methods. Fig. 2(a) shows the deblended data using the iterative f-x predictive filtering method (Chen et al., 2014). For simplicity, we use FX to refer to the f-x predictive filtering method from here. Fig. 2(b) shows the deblended data using the traditional SSA method. Fig. 2(c) shows the deblended data using the modified SSA method. Figs. 2(d), 2(e), and 2(f) show the zoomed profiles from Figs. 2(a), 2(b), and 2(c). From Fig. 2, it is clear that the FX method causes most residual noise while the proposed method obtains the cleanest result. The zoomed comparison gives a very

obvious demonstration on that the proposed method almost removes all the blending interference but the other two methods fail in removing enough noise. We then show the removed blending noise in Fig. 3. The removed noise section is calculated by subtracting the deblended data from the blended data, as shown in Fig. 1(b). From the comparison of blending noise, we can conclude that the FX method damages the most useful signals since there is a lot of spatially coherent energy shown in Fig. 3(a). The SSA method remove less useful energy than the FX method but more than the modified SSA method. We then calculate the deblending error sections and show them in Fig. 4. The deblending error is defined as the difference between the clean unblended data (the exact solution) and the deblended data. A successful deblending algorithm should make the deblending error close to zero. From the deblending error comparison as shown in Fig. 4, we can confirm the fact that the proposed causes least error but the FX method causes the most. Fig. 5 shows the SNR diagrams during the iterations. It is clear that the proposed method outperforms the other two methods in faster convergence and better converged SNR. For compare the amplitude details of different deblending methods, we show a trace-by-trace comparison in Fig. 6, where the 30-th trace from the unblended data (Fig. 1(a)), blended data (Fig. 1(b)), and the deblended data using three different methods (Figs. 2(a), 2(b), and 2(c)), are extracted and compared together. The trace-by-trace comparison confirms again that the proposed method obtains the result that is closest to the exact solution.

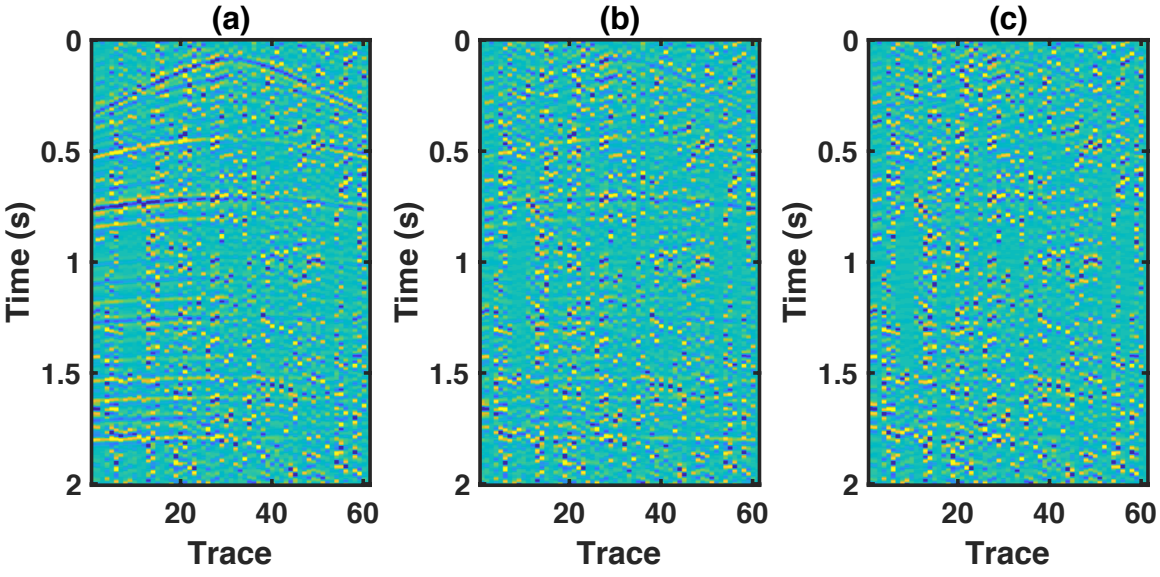

Fig. 3. Synthetic example. (a) Removed blending noise using FX method. (b) Removed blending noise using SSA method. (c) Removed blending noise using the proposed method. Note that the proposed method causes the least damages to the useful signals.

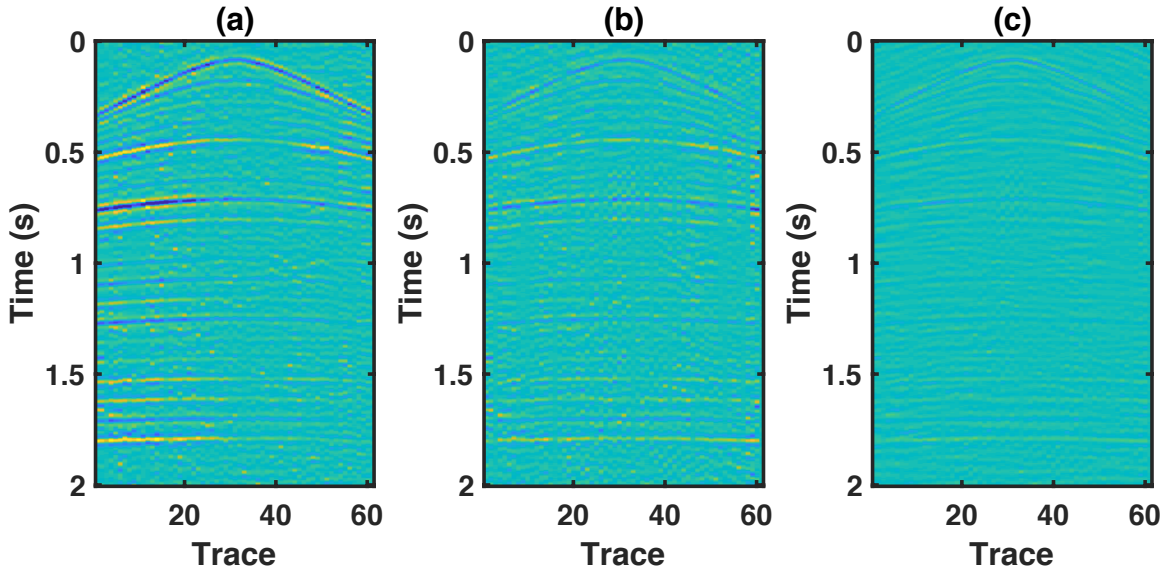

Fig. 4. Synthetic example. (a) Deblending error using FX method. (b) Deblending error using SSA method. (c) Deblending error using the proposed method. Note that the proposed method obtains the least deblending error.

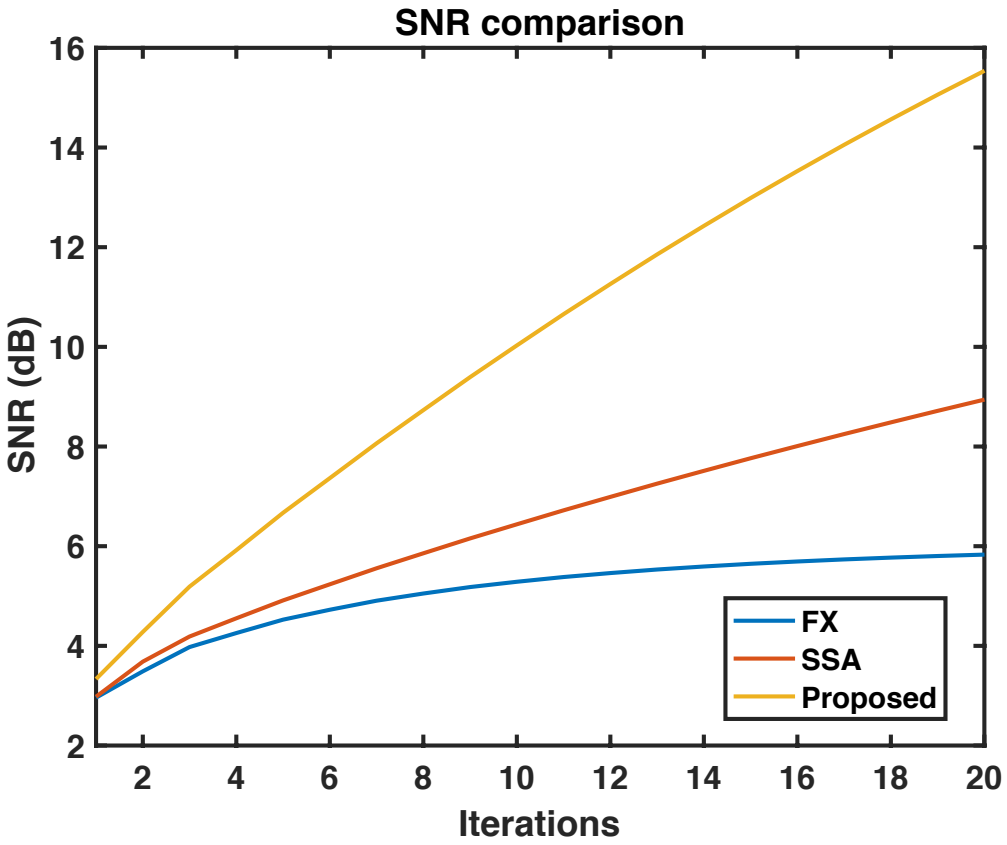

Fig. 5. Convergence diagram of the synthetic example in terms of SNR.

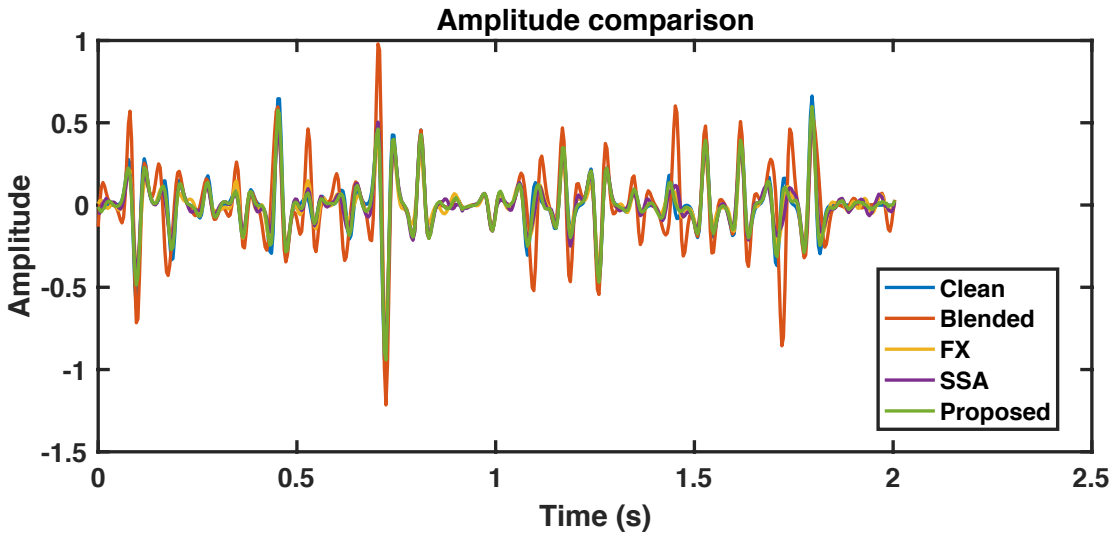

Fig. 6. Trace-by-trace amplitude comparison of the synthetic example. Note that the proposed method obtains the closest trace to the clean data.

We then test the proposed method on a real dataset. The unblended common receiver gather is shown in Fig. 7(a). Fig. 7(b) shows the corresponding blended data. The blending scheme and iterative solver to the inverse problem is exactly the same as the last example. Figs. 7(c) and 7(d) show two zoomed sections from the unblended and blended data, respectively. The blending noise in this example is even stronger than that in the last example. Fig. 8 show the deblending performance for three different methods. In this example, it seems that all three methods obtain much encouraging results since most blending noise has been removed. However, a detailed observation can find that there is much more residual noise in the deblended data using the FX and SSA methods than in the deblended data using the modified SSA method. It is worth mentioning that there is a lot of scattering interference before the first breaks in Figs. 8(a) and 8(b). The modified TSVD operation helps mitigate this type of noise and makes the resulted data smoother and cleaner, as shown in Fig. 8(c). The comparison among those zoomed sections shown in Figs. 8(d)-8(f) demonstrates that the modified SSA method removes more noise while maintaining the spatial coherency. Fig. 9 shows a comparison between the removed noise. Both traditional SSA and modified SSA methods do not remove too much useful energy, but the FX method does. There is a significant amount of useful energy shown in Fig. 9(a), which indicates that the FX method tends to lose energy during iterative inversion. There is a negligible amount of useful energy left in Fig. 9(b), which comes from the traditional SSA method. The proposed method causes almost no leakage useful energy and is thought to obtain the best performance. Fig. 10 shows a comparison of deblending error sections using different methods, which is consistent with the afore-mentioned observations and further confirms the superior performance from the proposed method. The SNR diagrams of this test is shown in Fig. 11.

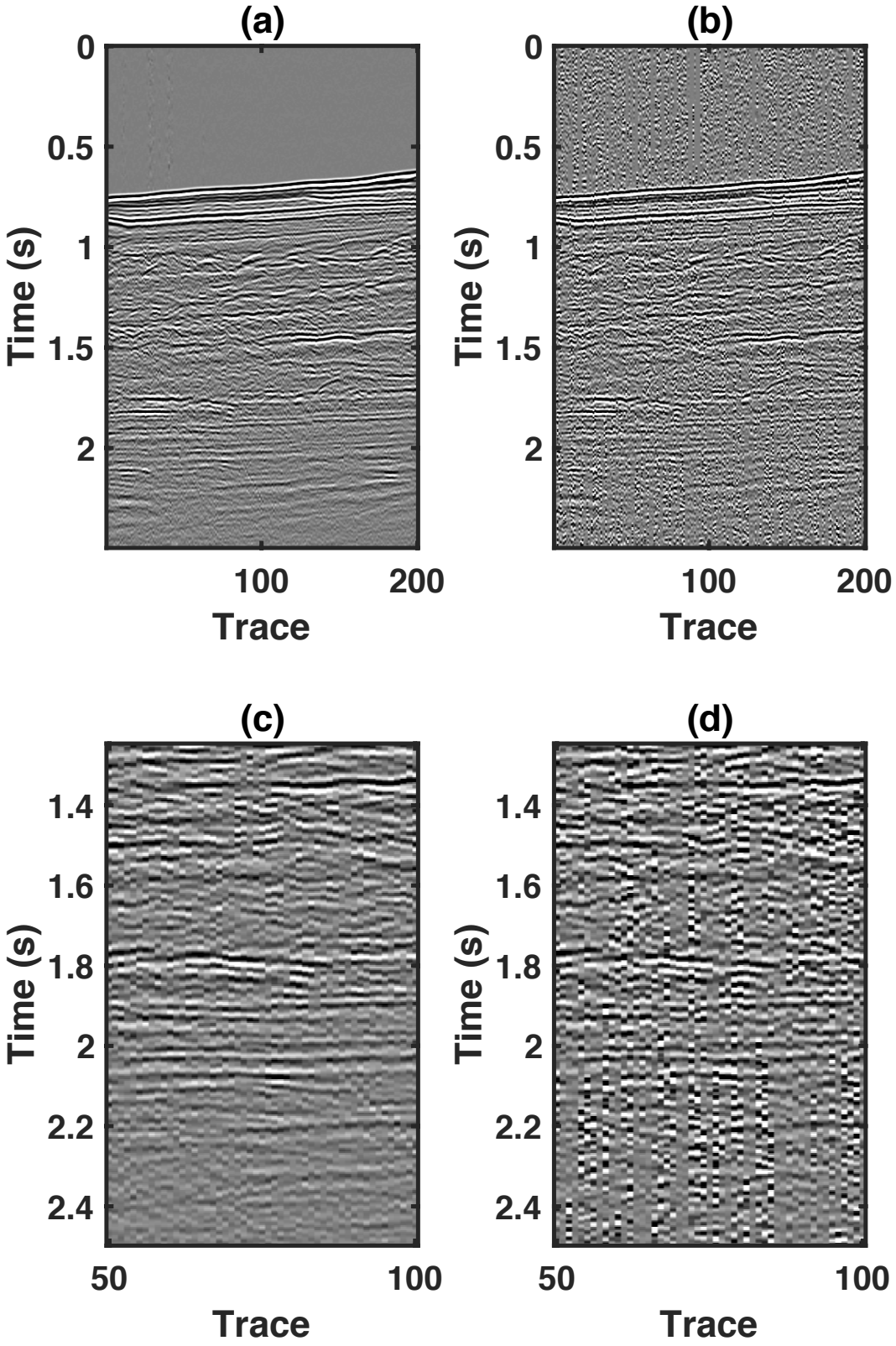

Fig. 7. Field data example. (a) Clean data. (b) Blended data. (c) Zoomed (a). (d) Zoomed (b).

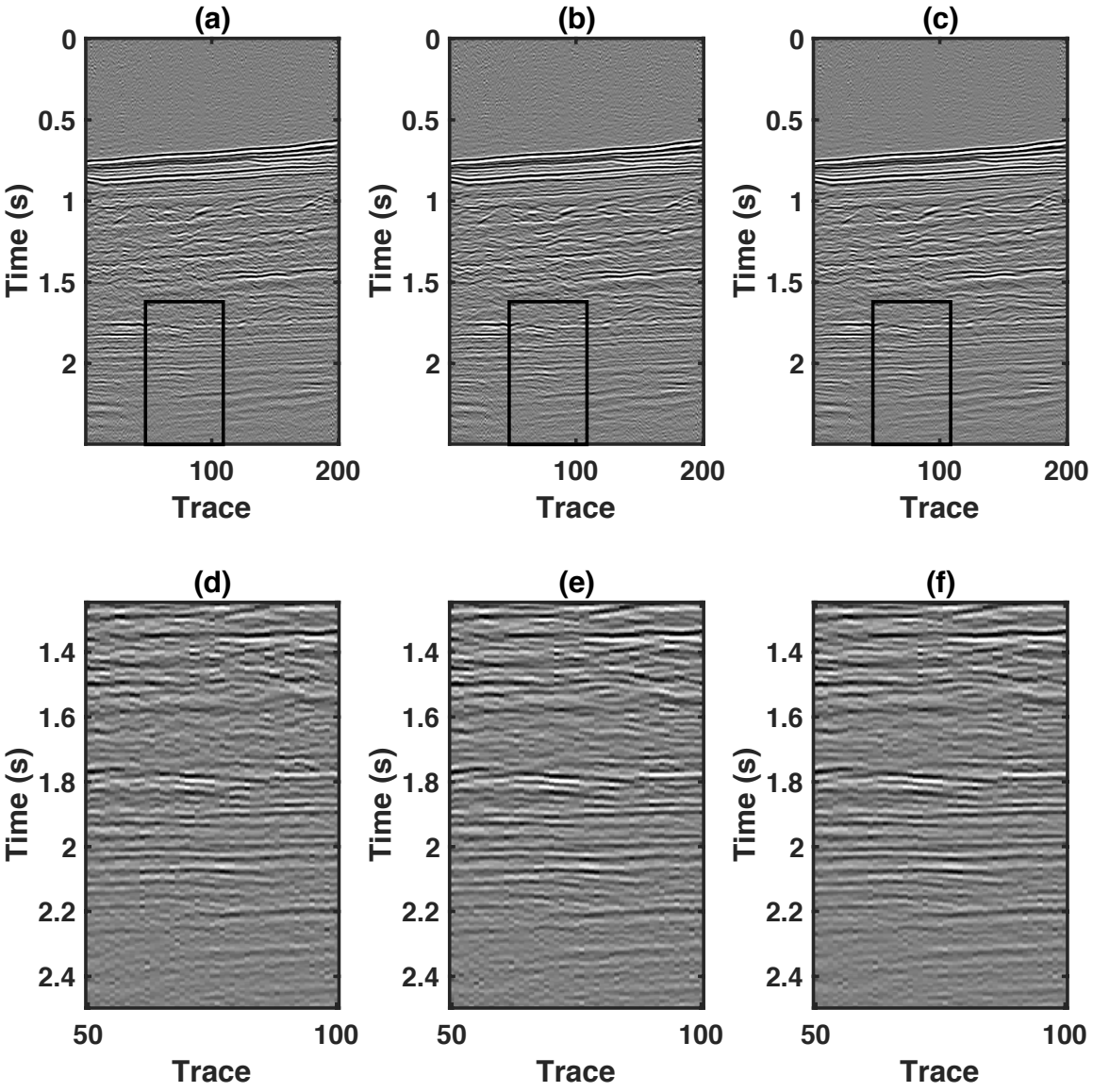

Fig. 8. Field data example. (a) Deblended data using FX method. (b) Deblended data using SSA method. (c) Deblended data using the proposed method. (d)-(f) Zoomed areas corresponding to the frameboxes in (a)-(c). Note that the proposed method obtains the cleanest result.

CONCLUSIONS

We have proposed a modified singular spectrum analysis (SSA) method for removing interferences caused from the simultaneous source acquisition. The traditional SSA method utilize the truncated singular value decomposition (TSVD) algorithm to separate the Hankel matrix into signal and noise components. In the modified SSA method, the TSVD is substituted with a more powerful modified TSVD algorithm, which can help better decomposing the data into signal and noise subspaces. The modified

SSA method can significantly improve the signal-and-noise separability during iterative inversion, which brings a much stronger deblending ability for the presented method. The proposed method is easy to be implemented and can be conveniently transformed into industrial applications. The synthetic and field data examples demonstrate the great potential of the proposed method in deblending.

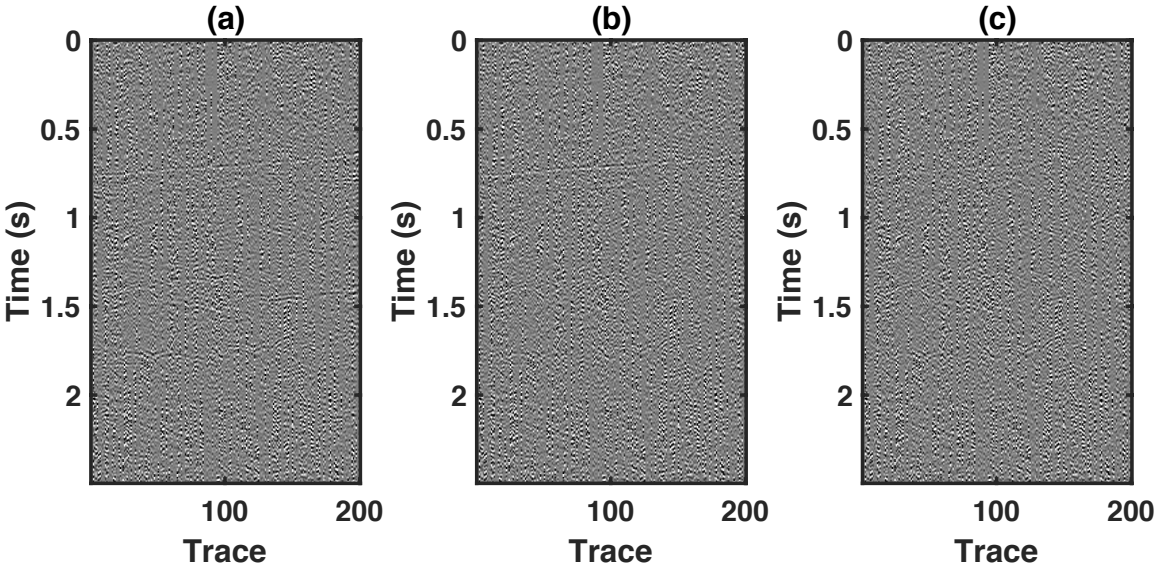

Fig. 9. Field data example. (a) Removed blending noise using FX method. (b) Removed blending noise using SSA method. (c) Removed blending noise using the proposed method. Note that the proposed method causes the least damages to the useful signals.

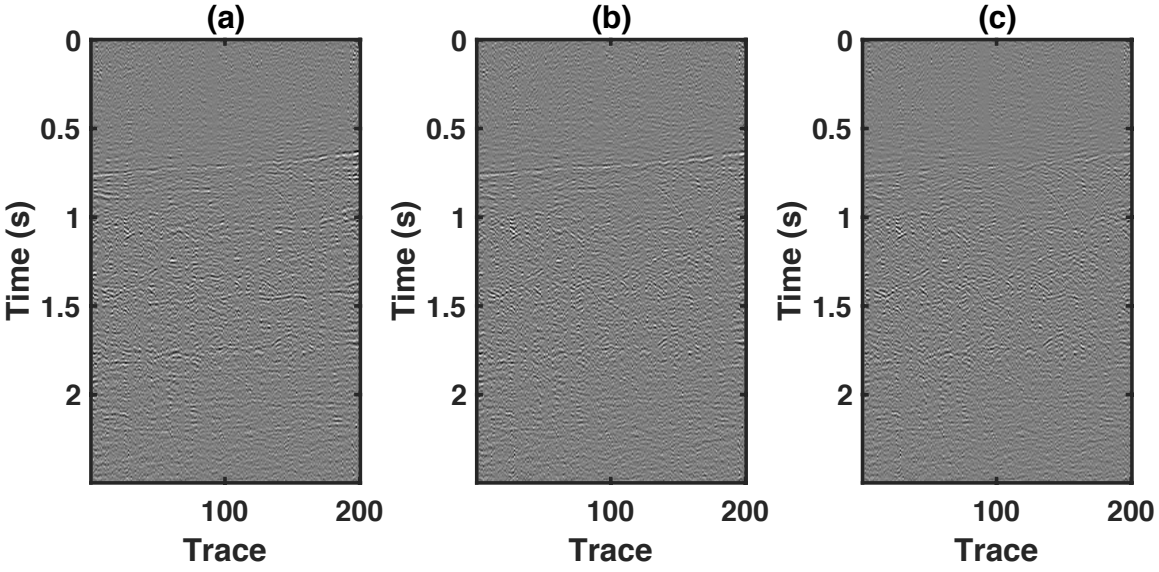

Fig. 10. Field data example. (a) Deblending error using FX method. (b) Deblending error using SSA method. (c) Deblending error using the proposed method. Note that the proposed method obtains the least deblending error.

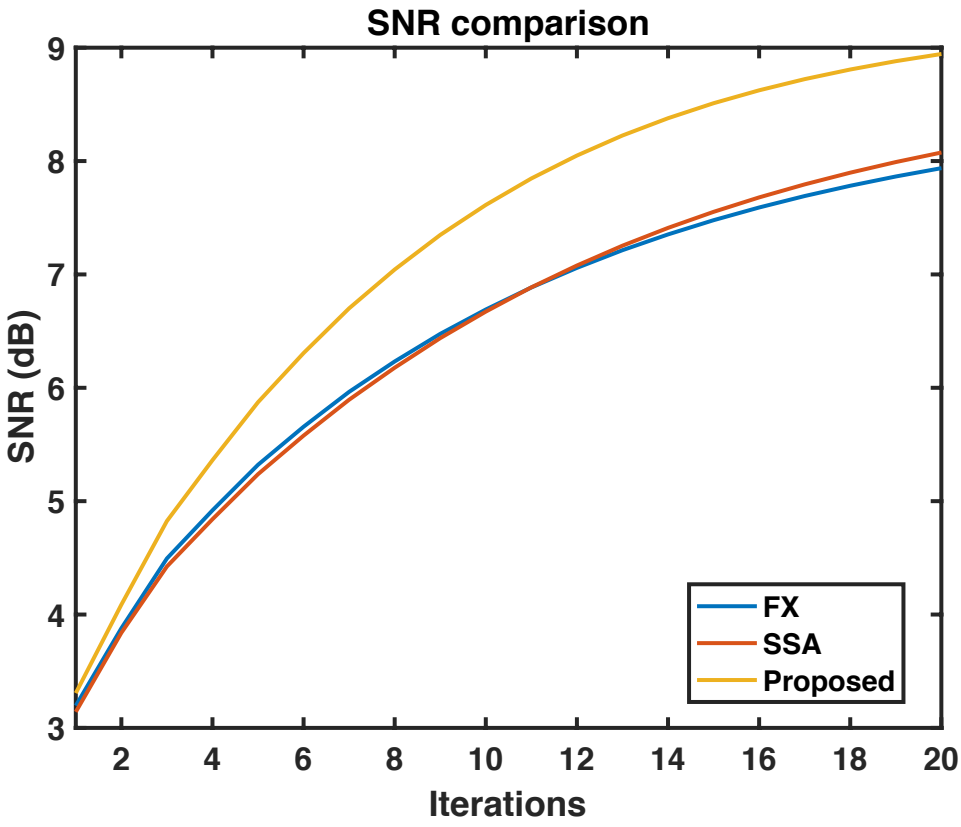

Fig. 11. Convergence diagram of the field data in terms of SNR.

ACKNOWLEDGEMENTS

The project is supported by the National Natural Science Foundation of China (Grant No. 41704121) and the starting fund at North China University of Water Resources and Electric Power (Grant No. 201705002, 201705003).

REFERENCES

Abma, R., 2014. Shot scheduling in simultaneous shooting. Expanded Abstr., 84th Ann. Internat. SEG Mtg., Denver: 94-98.

Abma, R.L. and Yan, J., 2009. Separating simultaneous sources by inversion. Extended Abstr., 71st EAGE Conf., Amsterdam.

Amundsen, L., Andersson, F., van Manen, D.-J., Robertsson, J.O. and Eggenberger K., 2018. Multi-source encoding and decoding using the signal apparition technique. Geophysics, 83: V49-V59.

Bai, M. and Wu, J., 2017. Efficient deblending using median filtering without correct normal moveout - with comparison on migrated images. J. Seismic Explor., 26: 455-479.

Bai, M. and Wu, J., 2018. Seismic deconvolution using iteartive transform-domain sparse inversion. J. Seismic Explor., 27: 103-116.

Bai, M., Wu, J., Xie, J. and Zhang, D., 2018. Least-squares reverse time migration of blended data with low-rank constraint along structural direction. J. Seismic Explor., 27: 29-48.

Beasley, C. J., 2008. A new look at marine simultaneous sources. The Leading Edge, 27: 914-917.

Berkhout, A.J., 2008. Changing the mindset in seismic data acquisition. The Leading Edge, 27: 924-938.

Berkhout, A.J. and Blacquière, G., 2013. Effect of noise in blending and deblending. Geophysics, 78(5): A35-A38.

Cadzow, J.A., 1988. Signal enhancement - a composite property mapping algorithm. IEEE Transact. Acoust., Speech, Sign. Process., 1: 49-62.

Chen, W., Chen, Y. and Cheng, Z., 2017a. Seismic time-frequency analysis using an improved empirical mode decomposition algorithm. J. Seismic Explor., 26: 367-380.

Chen, W., Chen, Y. and Liu, W., 2016a. Ground roll attenuation using improved complete ensemble empirical mode decomposition. J. Seismic Explor., 25: 485-495.

Chen, W., Xie, J., Zu, S., Gan, S. and Chen, Y., 2017b. Multiple reflections noise attenuation using adaptive randomized-order empirical mode decomposition. IEEE Geosci. Remote Sens. Lett., 14: 18-22.

Chen, W., Yuan, J., Chen, Y. and Gan, S., 2017c. Preparing the initial model for iterative deblending by median filtering. J. Seismic Explor., 26: 25-47.

Chen, W., Zhang, D. and Chen, Y., 2017d. Random noise reduction using a hybrid method based on ensemble empirical mode decomposition. J. Seismic Explor., 26: 227-249.

Chen, Y., 2016. Dip-separated structural filtering using seislet thresholding and adaptive empirical mode decomposition based dip filter. Geophys. J. Internat., 206: 457-469.

Chen, Y., 2017. Fast dictionary learning for noise attenuation of multidimensional seismic data. Geophys. J. Internat., 209: 21-31.

Chen, Y., 2018. Non-stationary least-squares complex decomposition for microseismic noise attenuation. Geophys. J. Internat., 213: 1572-1585.

Chen, Y., Chen, H., Xiang, K. and Chen, X., 2016b. Geological structure guided well log interpolation for high-fidelity full waveform inversion. Geophys. J. Internat., 207: 1313-1331.

Chen, Y., Chen, H., Xiang, K. and Chen, X., 2017e. Preserving the discontinuities in least-squares reverse time migration of simultaneous-source data. Geophysics, 82(3): S185–S196.

Chen, Y. and Fomel, S., 2015. Random noise attenuation using local signal-and-noise orthogonalization. Geophysics, 80(6): WD1-WD9.

Chen, Y. and Fomel, S., 2018. EMD-seislet transform. Geophysics, 83(1): A27-A32.

Chen, Y., Fomel, S. and Hu, J., 2014. Iterative deblending of simultaneous-source seismic data using seislet-domain shaping regularization. Geophysics, 79(5): V179-V189.

Chen, Y. and Ma, J., 2014. Random noise attenuation by f-x empirical mode decomposition predictive filtering. Geophysics, 79: V81–V91.

Chen, Y., Zhang, D., Huang, W. and Chen, W., 2016c. An open-source matlab code package for improved rank-reduction 3D seismic data denoising and reconstruction. Comput. Geosci., 95: 59-66.

Chen, Y., Zhang, D., Jin, Z., Chen, X., Zu, S., Huang, W. and Gan, S., 2016d. Simultaneous denoising and reconstruction of 5D seismic data via damped rank-reduction method. Geophys. J. Internat., 206: 1695-1717.

Doulgeris, P., Bube, K., Hampson, G. and Blacquière, G., 2012. Convergence analysis of a coherency-constrained inversion for the separation of blended data. Geophys. Prosp., 60: 769-781.

Fomel, S., 2007. Shaping regularization in geophysical-estimation problems. Geophysics, 72(2): R29-R36.

Fomel, S., 2008. Nonlinear shapping regularization in geophysical inverse problems. Expanded Abstr., 78th Ann. Internat. SEG Mtg., Las Vegas: 2046-2051.

Gan, S., Wang, S., Chen, Y. and Chen, X., 2016a. Simultaneous-source separation using iterative seislet-frame thresholding. IEEE Geosci. Remote Sens. Lett., 13: 197-201.

Gan, S., Wang, S., Chen, Y., Chen, X., Huang, W. and Chen, H., 2016b. Compressive sensing for seismic data reconstruction via fast projection onto convex sets based on seislet transform. J. Appl. Geophys., 130:194-208.

Gan, S., Wang, S., Chen, Y., Chen, X. and Xiang, K., 2016c. Separation of simultaneous sources using a structural-oriented median filter in the flattened dimension. Comput. Geosci., 86: 46-54.

Gan, S., Wang, S., Chen, Y., Qu, S. and Zu, S., 2016d. Velocity analysis of simultaneous-source data using high-resolution semblance-coping with the strong noise. Geophys. J. Internat., 204: 768-779.

Gan, S., Wang, S., Chen, Y., Zhang, Y. and Jin, Z., 2015. Dealiased seismic data interpolation using seislet transform with low-frequency constraint. IEEE Geosci. Remote Sens. Lett., 12: 2150-2154.

Huang, W., Wang, R. and Chen, Y., 2018a. Regularized non-stationary morphological reconstruction algorithm for weak signal detection in micro-seismic monitoring: Methodology. Geophys. J. Internat., 213: 1189-1211.

Huang, W., Wang, R., Chen, Y, Li, H. and Gan, S., 2016. Damped multichannel singular spectrum analysis for 3D random noise attenuation. Geophysics, 81(4): V261-V270.

Huang, W., Wang, R., Gong, X. and Chen, Y., 2018b. Iterative deblending of simultaneous-source seismic data with structuring median constraint. IEEE Geosci. Remote Sens. Lett., 15. doi: 10.1109/LGRS.2017.2772857.

Huang, W., Wang, R., Li, H. and Chen, Y., 2017a. Unveiling the signals from extremely noisy microseismic data for high-resolution hydraulic fracturing monitoring. Scientif. Rep., 7: 11996.

Huang, W., Wang, R., Yuan, Y., Gan, S. and Chen, Y., 2017b. Signal extraction using randomized-order multichannel singular spectrum analysis. Geophysics, 82: V59-V74.

Huang, W., Wang, R., Zhang, D., Zhou, Y., Yang, W. and Chen, Y., 2017c. Mathematical morphological filtering for linear noise attenuation of seismic data. Geophysics, 82: V369-V384.

Huang, W., Wang, R., Zhang, M., Chen, Y. and Yu, J., 2015. Random noise attenuation for 3D seismic data by modified multichannel singular spectrum analysis. Extended Abstr., 77th EAGE Conf., Madrid. doi: 10.3997/2214– 4609.201412830.

Huang, W., Wang, R., Zu, S. and Chen, Y., 2017d. Low-frequency noise attenuation in seismic and microseismic data using mathematical morphological filtering. Geophys. J. Internat., 211: 1318-1340.

Li, H., Wang, R., Cao, S., Chen, Y. and Huang, W., 2016a. A method for low-frequency noise suppression based on mathematical morphology in microseismic monitoring. Geophysics, 81(3): V159-V167.

Li, H., Wang, R., Cao, S., Chen, Y., Tian, N. and Chen, X., 2016b. Weak signal detection using multiscale morphology in microseismic monitoring. J. Appl. Geophys., 133: 39-49.

Liu, W., Cao, S. and Chen, Y., 2016a. Seismic time-frequency analysis via empirical wavelet transform. IEEE Geosci. Remote Sens. Lett., 13: 28-32.

Liu, W., Cao, S., Gan, S., Chen, Y., Zu, S. and Jin, Z., 2016b. One-step slope estimation for dealiased seismic data reconstruction via iterative seislet thresholding. IEEE Geosci. Remote Sens. Lett., 13: 1462-1466.

Liu, W., Cao, S., Jin, Z., Wang, Z. and Chen, Y., 2018. A novel hydrocarbon detection approach via high-resolution frequency-dependent avo inversion based on variational mode decomposition. IEEE Transact. Geosci. Remote Sens., 56: 2007-2024.

Mahdad, A., 2012. Deblending of Seismic Data. Ph.D. thesis, Delft University of Technology.

Mueller, M.B., Halliday, D.F., van Manen, D.-J. and Robertsson, J.O., 2015. The benefit of encoded source sequences for simultaneous source separation. Geophysics, 80(5): V133-V143.

Qu, S., Zhou, H., Chen, H., Zu, S. and Zhi, L., 2014. Separation of simultaneous vibroseis data. Expanded Abstr., 84th Ann. Internat. SEG Mtg., Denver: 4340-4344.

Qu, S., Zhou, H., Chen, Y., Yu, S., Zhang, H., Yuan, J., Yang, Y. and Qin, M., 2015. An effective method for reducing harmonic distortion in correlated vibroseis data. J. Appl. Geophys., 115: 120-128.

Qu, S., Zhou, H., Liu, R., Chen, Y., Zu, S., Yu, S., Yuan, J. and Yang, Y., 2016. Deblending of simultaneous-source seismic data using fast iterative shrinkage-thresholding algorithm with firm-thresholding. Acta Geophys., 64: 1066-1092.

Siahsar, M.A.N., Abolghasemi, V. and Chen, Y., 2017a. Simultaneous denoising and interpolation of 2D seismic data using data-driven non-negative dictionary learning. Sign. Process., 141: 309-321.

Siahsar, M.A.N., Gholtashi, S., Kahoo, A.R., Chen, W. and Chen, Y., 2017b. Data-driven multi-task sparse dictionary learning for noise attenuation of 3D seismic data. Geophysics, 82(6): V385-V396.

Siahsar, M.A.N., Gholtashi, S., Olyaei, E., Chen, W. and Chen, Y., 2017c. Simultaneous denoising and interpolation of 3D seismic data via damped data-driven optimal singular value shrinkage. IEEE Geosci. Remote Sens. Lett., 14: 1086-1090.

Verschuur, D.J. and Berkhout, A.J., 2011. Seismic migration of blended shot records with surface-related multiple scattering. Geophysics, 76(1): A7-A13.

Wang, Y., Zhou, H., Zu, S., Mao, W. and Chen, Y., 2017. Three-operator proximal splitting scheme for 3D seismic data reconstruction. IEEE Geosci. Remote Sens. Lett., 14: 1830-1834.

Wu, J. and Bai, M., 2018. Incoherent dictionary learning for reducing crosstalk noise in least-squares reverse time migration. Comput. Geosci., 114: 11-21.

Wu, S., Blacquière, G. and van Groenestijn, G.-J., 2015. Shot repetition: An alternative approach to blending in marine seismic. Expanded Abstr., 85th Ann. Internat. SEG Mtg., New Orleans: 48-52.

Xie, J., Chen, W., Zhang, D., Zu, S. and Chen, Y., 2017. Application of principal component analysis in weighted stacking of seismic data. IEEE Geosci. Remote Sens. Lett., 14: 1213-1217.

Xue, Y., Chang, F., Zhang, D. and Chen, Y., 2016. Simultaneous sources separation via an iterative rank-increasing method. IEEE Geosci. Remote Sens. Lett., 13, 1915-1919.

Xue, Y., Man, M., Zu, S., Chang, F. and Chen, Y., 2017. Amplitude-preserving iterative deblending of simultaneous source seismic data using high-order Radon transform. J. Appl. Geophys., 139: 79-90.

Yu, Z., Abma, R., Etgen, J. and Sullivan, C., 2017. Attenuation of noise and simultaneous source interference using wavelet denoising. Geophysics, 82: V179-V190.

Zhang, D., Chen, Y., Huang, W. and Gan, S., 2016. Multi-step damped multichannel singular spectrum analysis for simultaneous reconstruction and denoising of 3D seismic data. J. Geophys. Engin., 13: 704-720.

Zhang, D., Zhou, Y., Chen, H., Chen, W., Zu, S. and Chen, Y., 2017. Hybrid rank-sparsity constraint model for simultaneous reconstruction and denoising of 3D seismic data. Geophysics, 82(5): V351-V367.

Zhou, Y., Li, S., Zhang, D. and Chen, Y., 2018. Seismic noise attenuation using an online subspace tracking algorithm. Geophys. J. Internat., 212: 1072-1097.

Zhou, Y., Shi, C., Chen, H., Xie, J., Wu, G. and Chen, Y., 2017. Spike-like blending noise attenuation using structural low-rank decomposition. IEEE Geosci. Remote Sens. Lett., 14: 1633-1637.

Zu, S., Zhou, H., Chen, H., Zheng, H. and Chen, Y., 2017a. Two field trials for deblending of simultaneous source surveys: why we failed and why we succeeded? J. Appl. Geophys., 143: 182-194.

Zu, S., Zhou, H., Chen, Y., Pan, X., Gan, S. and Zhang, D., 2016a. Interpolating big gaps using inversion with slope constraint. IEEE Geosci. Remote Sens. Lett., 13: 1369-1373.

Zu, S., Zhou, H., Chen, Y., Qu, S., Zou, X., Chen, H. and Liu, R., 2016b. A periodically varying code for improving deblending of simultaneous sources in marine acquisition. Geophysics, 81(3): V213-V225.

Zu, S., Zhou, H., Li, Q., Chen, H., Zhang, Q., Mao, W. and Chen, Y., 2017b. Shot-domain deblending using least-squares inversion. Geophysics, 82(4): V241-V256.

Zu, S., Zhou, H., Mao, W., Zhang, D., Li, C., Pan, X. and Chen, Y., 2017c. Iterative deblending of simultaneous-source data using a coherency-pass shaping operator. Geophys. J. Internat., 211: 541-557.